



Article

# A Realistic Full-Scale 3D Modeling of Turning Using Coupled Smoothed Particle Hydrodynamics and Finite Element Method for Predicting Cutting Forces

Nishant Ojal <sup>1,\*</sup>, Ryan Copenhaver <sup>2</sup>, Harish P. Cherukuri <sup>3</sup>, Tony L. Schmitz <sup>2</sup>, Kyle T. Devlugt <sup>1</sup>  
and Adam W. Jaycox <sup>1</sup>

- <sup>1</sup> Precision Systems & Manufacturing, Lawrence Livermore National Laboratory, Livermore, CA 94550-9234, USA; devlugt1@llnl.gov (K.T.D.); jaycox1@llnl.gov (A.W.J.)  
<sup>2</sup> Department of Mechanical, Aerospace, and Biomedical Engineering, The University of Tennessee, Knoxville, TN 37996-2210, USA; rcopenh1@vols.utk.edu (R.C.); tony.schmitz@utk.edu (T.L.S.)  
<sup>3</sup> Department of Mechanical Engineering and Engineering Science, The University of North Carolina at Charlotte, Charlotte, NC 28223-0001, USA; hcheruku@uncc.edu  
\* Correspondence: ojal1@llnl.gov

**Abstract:** Computational modelling is an effective technique for understanding the complex physics of machining. Large deformations, material separation, and high computational requirements are the key challenges faced while simulating machining. This work introduces a full-scale three-dimensional model of turning operations using a combined approach based on the Smoothed Particle Hydrodynamics (SPH) and Finite Element (FE) methods. By exploiting the advantages of each method, this approach leads to high-fidelity coupled SPH-FE machining models. Cutting forces and chip morphology are the primary results of interest. The machining models are validated with the results of turning experiments. Two-dimensional machining model underpredicts the cutting force and feed force by approximately 49% and 70%, respectively. Moreover, passive force cannot be predicted using the two-dimensional model. On the other hand, with the three-dimensional models developed in this manuscript, the difference between the total simulated force and experimentally measured force is ~17%. The chip morphologies correlate with experiments in terms of the direction of the chip movement and the “long” continuous chips observed while turning Al 6061. This work expands the realm of machining simulations from two-dimensional orthogonal machining or sectional three-dimensional model to a full-scale realistic simulation. The encouraging simulation results show the potential to study more complex phenomena, such as machining stability and tool path modulation.



**Citation:** Ojal, N.; Copenhaver, R.; Cherukuri, H.P.; Schmitz, T.L.; Devlugt, K.T.; Jaycox, A.W. A Realistic Full-Scale 3D Modeling of Turning Using Coupled Smoothed Particle Hydrodynamics and Finite Element Method for Predicting Cutting Forces. *J. Manuf. Mater. Process.* **2022**, *6*, 33. <https://doi.org/10.3390/jmmp6020033>

Academic Editor: Steven Y. Liang

Received: 19 February 2022

Accepted: 7 March 2022

Published: 11 March 2022

**Publisher's Note:** MDPI stays neutral with regard to jurisdictional claims in published maps and institutional affiliations.



**Copyright:** © 2022 by the authors. Licensee MDPI, Basel, Switzerland. This article is an open access article distributed under the terms and conditions of the Creative Commons Attribution (CC BY) license (<https://creativecommons.org/licenses/by/4.0/>).

**Keywords:** three-dimensional machining; orthogonal machining; Johnson–Cook constitutive model; smoothed particle hydrodynamics; finite element analysis

## 1. Introduction

With technological advancement, there is an increasing demand for high-quality products at low manufacturing costs and better process efficiency that requires a comprehensive study of the processes involved in manufacturing. Machining is one of the most common manufacturing operations to process raw material into a finished product. Understanding the complex physical phenomena occurring during machining is important for enhancing the product quality and reducing the operating cost.

Computational modelling is an important tool for understanding and optimizing machining operations. Many researchers have studied machining using the Finite Element Method (FEM). However, in the majority of the works, the FEM models were based on the assumption of two-dimensional plane-strain. This is because of the challenges associated with the FEM in modelling high deformation, material separation, and contact during

machining. Due to these disadvantages associated with FEM, the Smoothed Particle Hydrodynamics (SPH) method has attracted the attention of many researchers as an alternative to FEM. The SPH method is a Lagrangian, particle-based, meshless method. It has several advantages over the grid-based approaches. High strains occurring in machining are easily modelled due to the meshless nature of the method. Particles undergoing deformation move without any topological restrictions. Furthermore, a separation model or contact model is not required in the SPH method. The relative motion of the particles with respect to each other and with respect to the tool surface allows for the “natural” chip-workpiece separation.

In this work, the turning operation of a cylindrical workpiece is simulated using a full-scale three-dimensional model. A coupled SPH-FE method is used for modelling. Coupling of the SPH method with FEM utilizes the advantages of the SPH method for modelling material separation and high deformation zone and offsets the computationally expensive SPH method by the use of FE elements in low deformation zones and thereby reducing the simulation time. The force components in all three directions and the chip profile predicted by the simulation agree well with the experimental observations. In addition to predicting more realistic machining output, full-scale three-dimensional models enable a more complete understanding of machining through numerical simulations by incorporating complex phenomena such as machine dynamics and tool path modulations.

## 2. Literature Review

Machining has received much attention from researchers due to its widespread use in manufacturing of parts. Improvement of machining output through a better understanding of the relationship between input variables (such as tool geometry, material to be machined, etc.) and the output variables (such as cutting forces, temperature rise, tool wear, etc.) is the primary objective of the studies. Both experimental and numerical studies are being conducted to understand the complex phenomena that occur during machining. However, Sadeghifar et al. [1] state several difficulties associate with experimental studies, such as difficulty in measuring physical quantities in the cutting zone. Ivester and Kennedy [2], while conducting a series of machining experiments, described the shortcoming of measuring temperatures, especially at the tool–chip interface.

Finite Element Method is a numerical technique commonly used for modelling machining. Arrazola et al. [3] have summarized the state-of-the-art developments in modelling of machining processes. Besides presenting the advancements in computational approaches, an urgent need to move from 2D to 3D model development is identified to meet the industry needs. Primarily, three approaches are used for the computational modelling of machining, namely Lagrangian, Eulerian and Arbitrary Lagrangian–Eulerian (ALE) approaches. In the Lagrangian approaches, the mesh deforms with the material. In the Eulerian approaches, the mesh is fixed in space and material enters and exits the space through a predefined boundary. An ALE approach combines the unique features of both the Lagrangian and Eulerian formulations. In the Lagrangian approach, researchers have used widely different models for simulating chip separation from the workpiece on a prior prescribed chip separation path. For example, Zhang and Bagchi [4] used a conditional link element and Mabrouki et al. [5] used accumulated equivalent inelastic deformation as the separation criterion. Carroll and Strenkowski [6] used the Eulerian approach used to simulate the cutting process. Steady state chip shape needs to be assigned before the simulation. Movahhedy et al. [7] used the ALE approach to model machining. However, Chenot et al. [8] noted that the effect on overall accuracy of the results requires a special attention due to the remapping step. Thus, depending on the approach used, challenges such as high mesh distortions, element deletion, prior prescription of chip separation path and remapping error are associated with the use of FEM.

The Smoothed Particle Hydrodynamics (SPH) method eliminates the disadvantages associated with the Finite Element Method because of the lack of physical connection between the particles used for discretizing the domain. Machining models using the SPH

method have been developed by various researchers. Limido et al. [9] presented a 2D orthogonal machining model using the SPH method. Johnson-Cook constitutive model is used to model the material behaviour of the workpiece. The SPH model is able to predict continuous chip for Al6061-T6 workpiece and shear localized chips for AISI4340 steel workpiece. The machining forces agree to within 10% and 30% of the measured values for tangential and normal components, respectively. He concluded that the SPH method is advantageous for machining modelling due to its meshless nature in terms of chip-workpiece natural separation and no requirement for remeshing. Villumsen and Fauerholdt [10] conducted sensitivity analysis for the influence of parameters such as particle resolution, time scaling, mass scaling and friction between tool and workpiece on the predicted cutting force. The cutting forces converged at low particle resolutions. While increasing tool velocity in model is recommended for reducing the simulation time, application of mass scaling resulted in the increase of cutting forces. Avachat and Cherukuri [11] conducted a parametric study of the three most important parameters, namely, the smoothing length, particle density and SPH formulation on chip morphology and stress distribution. These studies provide an insight into the numerical parameters associated with the SPH method. Xi et al. [12] presented a coupled SPH-FE machining model to study thermally-assisted machining of Ti6Al4V. Influence of the initial workpiece temperature on the chip formation and cutting force is studied. In this model, the zone of the workpiece interacting with the tool (high deformation zone) is discretized by SPH particles, and FE mesh is used in low deformation zone. Chip segmentation and cyclic cutting forces, typical of machining Ti6Al4V, were observed. A coupled SPH-FE model is also utilized by Song et al. [13] to study laser-assisted machining of fused silica and predict cutting forces and chip morphology. The application of the laser heating resulted in more continuous chips, reduction of cutting forces and improved surface finish.

Two-dimensional plane-strain, orthogonal machining models constitute the majority of the current studies. The predicted cutting forces align well with experiments. The experimental conditions used in these studies satisfy plane-strain condition assumptions. However, the feed forces are highly under-predicted. Mane et al. [14] observed a large difference between the experimentally measured and numerically predicted feed forces. Laakso et al. [15] conducted multiple machining simulations by changing the values of friction coefficient and tool geometry. He concluded that the tool wear during machining has the most significant effect on the feed force, followed by the friction coefficient. Calamaz et al. [16] observed that the best agreement between experimental and simulated feed forces is obtained for simulations with the highest values of the friction coefficient. Childs and Rahmad [17] even used the friction coefficient between the tool and the chip to values greater than 1 to correct this under-prediction of the feed force. Another limitation of using 2D models is that the passive forces cannot be predicted through these models.

Limited studies [18–23] have been conducted incorporating the more realistic three-dimensional machining models. Unlike the 2D orthogonal machining models, Llanos et al. [18] simulated oblique machining using a 3D machining model. The workpiece is modelled as a three dimensional cuboid shape. For validation, experimental observations of turning of a 3 mm thin wall tube is used. Variation of cutting forces obtained by FEM and experiments are compared qualitatively. This comparison is done for different input conditions such as varying friction, depth of cut, mass scaling and cutting tool geometry. Olleak and Özel [19] studied the effects of textured tool by modelling a 2 mm thin wall workpiece in three dimensions. Özel et al. [20] modelled a more realistic face turning operation using three-dimensional ALE Finite Element Method. However, in all these studies, only a section of the workpiece has been modelled. Although the simulated cutting forces may seem to be stabilize for a small workpiece, the actual cutting force can vary depending on the machining conditions. The machined surface, chip profile and resulting uncut chip thickness may vary for the subsequent revolutions of the workpiece. Moreover, industrial machining operations are predominantly three-dimensional in nature. Hence, to predict various field variables such as stresses, strains, and temperatures for these operations,

a more realistic three-dimensional machining model is needed. This work aims to predict all three components of the cutting forces and the chip morphology during machining by modelling a full-scale three-dimensional model of the workpiece. The results of the simulation are validated with experimental observations.

### 3. Smoothed Particle Hydrodynamics (SPH) Method

Smoothed particle hydrodynamics (SPH) is a meshfree, Lagrangian method introduced by Gingold and Monaghan [24] and Lucy [25] for astrophysical applications. Due to its advantages, the method is being increasingly used in solid and fluid mechanics problems. In this method, a body is discretized using particles. Each particle has an associated set of state variables. The particle interacts with the neighbouring particles which are within its domain of influence. The smoothing function acts as a weight for the neighbouring particles to approximate the state variables of the particle. The discretized conservation equations and constitutive equations are solved to obtain the time variation of the state variables. The method is described in detail in Liu and Liu [26], and also summarized in Feng et al. [27].

At the core of the SPH method is the kernel function. The kernel function smooths out the neighbouring particle's contribution to a property field based on distance from the respective particle. The influence of a neighbouring particle reduces with the increasing distance. The summation form of a property field  $f$  at position  $\mathbf{r}^a$  is given by

$$\langle f(\mathbf{r}^a) \rangle = \sum_{b=1}^N W(\mathbf{r}^{ab}, h) f(\mathbf{r}^b) \frac{m^b}{\rho^b} . \tag{1}$$

Here,  $W(\mathbf{r}^{ab}, h)$  is the smoothing function,  $\mathbf{r}^{ab} = |\mathbf{r}^a - \mathbf{r}^b|$  is the distance of neighbouring particle at position  $\mathbf{r}^b$  from the particle at  $\mathbf{r}^a$ ,  $h$  is called smoothing length,  $\rho_b$  is the density of particle and  $m_b$  is the mass of the particle at position  $\mathbf{r}^b$ . The value of a property at a point is calculated using the summation of the values of the property at the neighbouring particles, weighted by the kernel function, as illustrated in Figure 1.

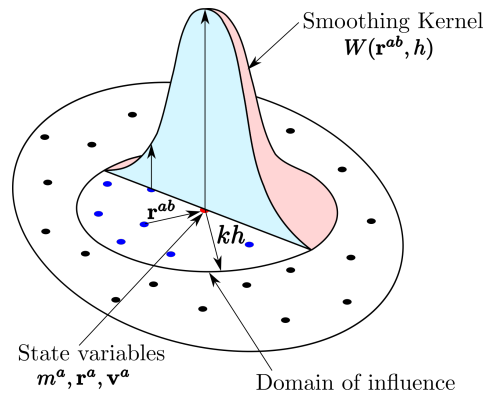


**Figure 1.** A schematic of a smoothing kernel function. Smoothing kernel function provides weighted contribution of neighbouring particles during the calculation of property at a point.

#### 3.1. Discrete Form of Conservation Laws

The conservation laws are discretized using Equation (1). The conservation of mass in summation approximation is given by

$$\left\langle \frac{D\rho^a}{Dt} \right\rangle = \sum_{b=1}^N m^b (v_i^a - v_i^b) \frac{\partial W^{ab}}{\partial x_i^a} . \tag{2}$$

Here,  $\rho$  is the density,  $m$  is mass,  $\mathbf{v}$  is velocity and  $x_i$  are the co-ordinates.

Similarly, the conservation of linear momentum is given by

$$\left\langle \frac{Dv_i^a}{Dt} \right\rangle = \sum_{b=1}^N m^b \left( \frac{\sigma_{ij}^a}{(\rho^a)^2} + \frac{\sigma_{ij}^b}{(\rho^b)^2} - \Pi_{ij} \right) \frac{\partial W^{ab}}{\partial x_j^a} . \tag{3}$$

Here,  $\sigma$  is the total stress tensor and  $\Pi_{ij}$  is the artificial viscosity term accounting for numerical instability during discontinuity, for example, a shock. The forces acting on the particles during the simulation are calculated using the conservation of linear momentum. The angular momentum is conserved explicitly by the SPH formulation.

The conservation of energy is given by

$$\left\langle \frac{DU^a}{Dt} \right\rangle = \frac{1}{2} \sum_{b=1}^N m^b \left( \frac{p^a}{(\rho^a)^2} + \frac{p^b}{(\rho^b)^2} \right) v_j^{ab} \frac{\partial W^{ab}}{\partial r_j^a} + \frac{\mu^a}{2\rho^a} \varepsilon_{ij}^a \varepsilon_{ij}^a + \left\langle Q_i \right\rangle . \tag{4}$$

Here,  $U$  is internal energy per unit mass,  $p$  is isotropic pressure component of the total stress tensor  $\sigma$ ,  $\mu$  is dynamic viscosity,  $\varepsilon$  is the shear strain-rate and  $Q$  is the rate of thermal energy per unit mass.

### 3.2. Equation of State

The equation of state (EOS) determines pressure  $p$  as a function of local density  $\rho$  and other material property variables. For machining simulations, Mie-Grüneisen equation has been widely used and is given by the following equations [28]. For compression ( $\mu > 0$ ),

$$p = \frac{\rho_0 C^2 \mu \left[ 1 + \left( 1 - \frac{\gamma_0}{2} \right) \mu - \frac{b}{2} \mu^2 \right]} \left[ 1 - (S_1 - 1) \mu - S_2 \frac{\mu^2}{\mu + 1} - S_3 \frac{\mu^3}{(\mu + 1)^2} \right]^2 + (\gamma_0 + b\mu)e , \tag{5}$$

and for tension ( $\mu < 0$ ),

$$p = \rho_0 C^2 \mu + (\gamma_0 + b\mu)e . \tag{6}$$

Here,  $C$  is the bulk speed of sound,  $\mu = \rho/\rho_0 - 1$ ,  $\rho$  is the current density,  $\rho_0$  is the reference density,  $\gamma_0$  is Grüneisen gamma,  $S_1, S_2$  and  $S_3$  are the Hugoniot slope coefficients,  $b$  is the first order volume correction to  $\gamma_0$ , and  $e$  is the internal energy per initial volume. The parameters  $C, \gamma_0, S_1, S_2, S_3$  and  $b$  define the EOS of the material.

### 3.3. Material Model

The inelastic behaviour of the workpiece is modelled using the Johnson–Cook material model [29], given by

$$\sigma_{eq} = \underbrace{\left( A + B\varepsilon_p^n \right)}_{\text{Strain hardening}} \underbrace{\left[ 1 + C \ln \dot{\varepsilon}^* \right]}_{\text{Strain rate sensitivity}} \underbrace{\left[ 1 - T^{*m} \right]}_{\text{Thermal softening}} . \tag{7}$$

Here,  $\sigma_{eq}$  is flow stress of the material.  $A, B, n, C$  and  $m$  are material constants.  $\varepsilon_p$  is the equivalent plastic strain. The dimensionless strain rate,  $\dot{\varepsilon}^*$  is the ratio of the plastic strain-rate,  $\dot{\varepsilon}_p$  and reference strain rate,  $\dot{\varepsilon}_0$ . Furthermore, the homologous temperature,  $T^*$  is defined by

$$T^* = \frac{T - T_0}{T_m - T_0} . \tag{8}$$

Here,  $T, T_0$  and  $T_m$  are, respectively, the material temperature, reference temperature and melting temperature.

In addition to the constitutive material model, the Johnson–Cook damage model [29] is used to simulate failure and is given by

$$\varepsilon_f = [D_1 + D_2 \exp(D_3 \sigma^*)] [1 + D_4 \ln \dot{\varepsilon}^*] [1 + D_5 T^*] . \tag{9}$$

Here,  $\varepsilon_f$  is the equivalent fracture strain.  $D_1 - D_5$  are the damage model constants. The stress triaxiality parameter,  $\sigma^*$ , is a ratio of the mean stress,  $\sigma_m$ , and the equivalent stress,  $\sigma_{eq}$ . Fracture occurs when the cumulative value of the equivalent plastic strain equals  $\varepsilon_f$ . The damage of an element,  $D$ , is defined based on a cumulative damage law, represented by,

$$D = \sum \frac{\Delta \varepsilon_p}{\varepsilon_f} . \quad (10)$$

When  $D$  equals unity, fracture is assumed to occur. The stress tensor in the material undergoing deformation is given by the scalar damage equation,

$$\sigma_D = (1 - D)\sigma_{eq} . \quad (11)$$

It is noteworthy that the particles reaching equivalent fracture strain are deleted from the SPH calculations. However, the mass and energy of these particles are retained. This ensures conservation of mass. This is contrary to FEM, where the elements are completely deleted from the model due to high distortion, leading to loss of mass from the model.

#### 4. Machining Models

A two-dimensional machining model and a full-scale three-dimensional machining model are developed in this work using Ansys LS-DYNA<sup>®</sup> software. These models use a coupled SPH-FE mesh to discretize the workpiece. SPH particles are used in the zone of cutting, where the workpiece interacts with the tool. This is a zone of high deformation. The chip forms, curls and comes in contact with itself and the surface of the tool. Finite Element mesh is used away from this zone, where the deformation is low. SPH particles and FE mesh are coupled at the interface. This coupling allows for the smooth transfer of the physical properties, such as displacement and stress.

The coupling of SPH particles with FE mesh is accomplished by constraining the bottom layer of SPH particles with FE mesh by using the node to surface constraining algorithm. Here, the SPH elements are considered as slave part and the finite elements are considered as master part. The acceleration of each slave node is then interpolated from the master segment containing its contact points [30].

The coupled SPH-FE approach combines the benefits of both these methods. The challenges associated with using the FE method such as mesh distortions and material separation modelling are easily handled by the SPH method. Unlike element deletion of FE mesh in FEM to model high deformation and material separation, SPH particles move with respect to each other without any topological restrictions. This allows for the “natural” chip–workpiece separation during machining simulations.

At the same time, the high computational times associated with SPH method are reduced with the use of FE mesh in the low deformation zones. Thus, coupling of SPH and FE methods results in high-fidelity and numerically efficient models. In the following, the geometry, boundary conditions and material properties used in the models are presented.

##### 4.1. 2D Machining Model

Two-dimensional orthogonal modelling is a widely used approach for modelling machining. The workpiece is modelled as a two-dimensional rectangular domain. A plane-strain condition is assumed for this model. The geometry and the boundary conditions used in this model are shown in Figure 2. The tool is given a cutting velocity in the negative  $X$  direction and is completely constrained in all the other directions. The workpiece is fully constrained on the left and bottom sides. For plane-strain assumption, the motion of all the SPH particles and FEM elements of the workpiece and the tool is fully constrained in  $Z$  direction (normal to the plane). Mesh convergence of SPH particles and FE mesh is conducted based on the prior works [11,31]. The material properties used in this model are described in Section 4.2.2.

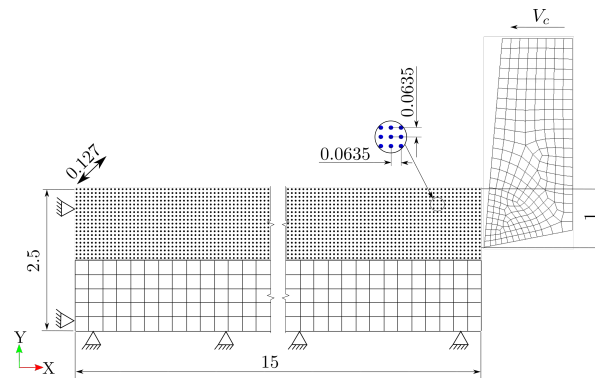


**Figure 2.** Two-dimensional machining model with geometry and boundary conditions.

#### 4.2. 3D Machining Model

Since machining is a three-dimensional process and two-dimensional models do not fully capture the physics of machining, a 3D machining model is developed. In addition to predicting the cutting forces in all the three directions, this model can simulate chip morphology during machining.

##### 4.2.1. Geometry and Mesh

The machining model, shown in Figure 3, consists of a tool and a cylindrical workpiece. The tool is discretized using a Finite Element mesh and the workpiece is discretized using a coupled SPH-FE mesh. The geometry and mesh of the tool and the workpiece are shown, respectively, in Figure 4a,b. All length dimensions are in mm.

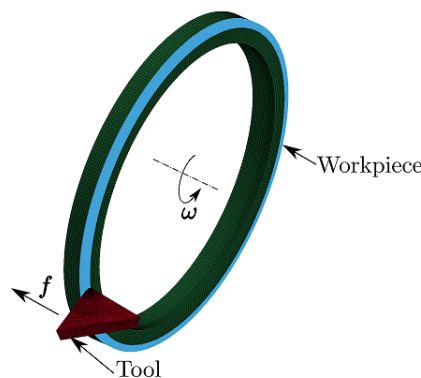


**Figure 3.** A coupled SPH-FE model of three-dimensional turning operation: Blue colour region of the workpiece is meshed using SPH particles, whereas green coloured region is meshed with FE mesh.

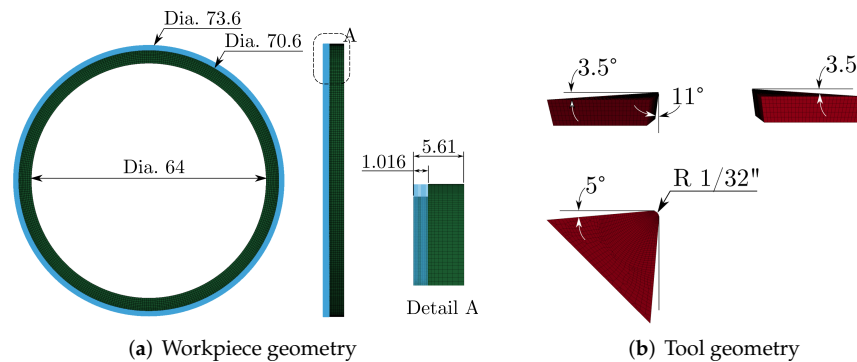


**Figure 4.** Geometry of workpiece and tool used for 3D machining model. Instead of modelling the complete tool, only the section involved in machining is modelled for the simulations.

### 4.2.2. Material Properties

The material of the tool is tungsten carbide, and that of the workpiece is Al 6061 (chemical composition shown in Table 1). The physical properties of the tool and the workpiece are shown in Table 2. The tool is modelled as a rigid body. This simplification is based on the fact that the tool is comparatively more rigid than the workpiece. For modelling, the workpiece and its fracture in the form of chips, the Johnson–Cook material model along with the Johnson–Cook damage model are used. The parameters of these material models are shown in Table 3.

**Table 1.** Chemical composition of workpiece (Al 6061) [32].

Element	Si	Fe	Cu	Mn	Mg	Cr	Zn	Sn	Al
Content %	0.4–0.8	0.7	0.15–0.4	0.15	0.8–1.2	0.04–0.35	0.25	0.15	remainder

**Table 2.** Physical properties of workpiece and tool [33].

Property	Workpiece	Tool
Density, $\rho$ (Kg/m <sup>3</sup> )	2700	11,900
Young’s Modulus, E (GPa)	68.9	534
Poisson’s ratio, $\nu$	0.33	0.22
Specific heat, $C_p$ (J/Kg K <sup>-1</sup> )	896	-
$T_{melt}$ , (K)	855	-
$T_{room}$ , (K)	300	300

**Table 3.** Johnson–Cook parameters of workpiece (Al 6061) [29,34].

Parameter	A (MPa)	B (MPa)	$n$	C	$m$
Value	324	114	0.42	0.002	1.34
Parameter	$D_1$	$D_2$	$D_3$	$D_4$	$D_5$
Value	-0.77	1.45	-0.47	0	1.6

### 4.2.3. Boundary Conditions

The boundary conditions are applied to the tool and the workpiece. All nodes of the tool are fully constrained in Y and Z directions. The cutting velocity,  $V_c$  is given to the tool in X direction. This velocity is calculated from the feed per revolution of the tool and the rotational speed of the workpiece. The boundary conditions on the workpiece are applied on the back face of the workpiece. All nodes on the back face are constrained to rotate along its centerline axis. Additionally, they are constrained for translation in X direction. The boundary conditions are shown in Figure 5.

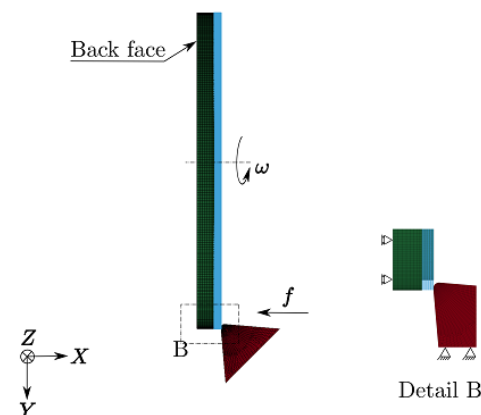


**Figure 5.** Boundary conditions applied in 3D machining model.

## 5. Machining Experimental Setup

A Haas TL-1 computer numerically controlled (CNC) lathe (8.9 kW, 2000 rpm spindle) is used for the experiments. Cylindrical workpieces of Al 6061 are dry machined with the prescribed depth of cut 1 mm, cutting speed of 800 SFM (1083 rpm) and feed rate of 0.254 mm/rev. The cutting tool used is Kennametal part number 1183375 (ANSI catalog number CPGN 120308 KC730). The tool geometry consists of 80° parallelogram carbide inserts with a positive 3.5° rake angle. The insert was replaced once the measured Flank Wear Width (FWW) value reached 0.3 mm [35,36] to prevent increased cutting forces due to a worn insert. FFW is the average width of the flank wear land,  $VB_B$  and was measured as per ISO 3685:1993 [37], using a Dinolite digital microscope and a measurement software. The setup is shown in Figure 6.

Dynamic cutting forces are measured using a three-axis dynamometer (Kistler 9257B), which is mounted on the lathe's cross slide. An infrared camera (FLIR E40) is attached to the cross slide to establish the temperature trends with changes in machining conditions. A laser vibrometer (Polytec OFV-534/OFV-5000) is used to measure the feed direction motion (Z direction) to verify the actual feed rate during machining. A digital microscope (not pictured) is used to measure insert flank wear at a fixed location between the machining tests.

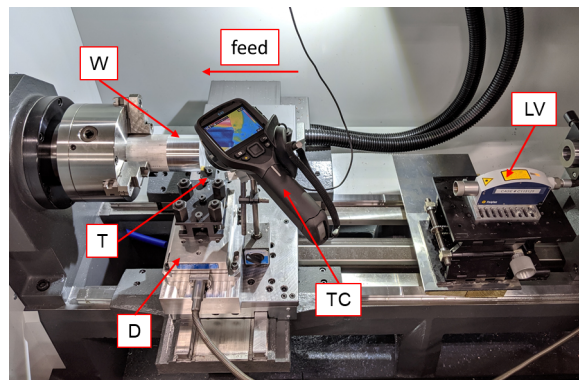


**Figure 6.** Photograph of turning setup including workpiece (W), dynamometer (D), cutting tool (T), thermal camera (TC), and laser vibrometer (LV).

## 6. Results

Results of the two-dimensional (2D) machining model and the three-dimensional (3D) machining model are presented in this section. The results of interest are the cutting forces and the chip morphology.

### 6.1. 2D Machining Simulation

Initially, the 2D machining model is simulated. Although the assumptions of the plane-strain conditions are not satisfied by the experimental conditions, the 2D machining models are simulated to quantify the deviation of cutting forces from the experimental values. The simulated chip profile (shown in Figure 7) is continuous, which is typically observed during the machining of Al 6061. A comparison of the simulated cutting forces with the experimental values is shown in Table 4. The cutting force is underpredicted by 49%. The feed force is highly underpredicted. This result is similar to the observations by various researchers, explained in detail in the literature review section. Additionally, the passive force cannot be predicted using the 2D model. Underprediction of 55% is observed in the total force, which is the result of all three force components.

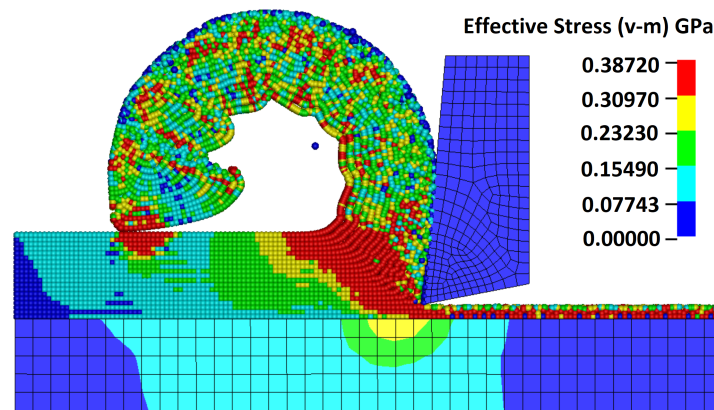


Figure 7. Simulated chip profile by 2D machining model.

Table 4. Comparison of forces predicted by 2D model with experiments.

	Experimental (N)	Simulated (N)
Feed Force ( $F_f$ )	100	-
Passive Force ( $F_p$ )	65	19
Cutting Force ( $F_c$ )	235	120
Total Force ( $F$ )	264	121

Based on the above result, it is evident that the 3D machining models are required to simulate the turning of cylindrical workpieces accurately. However, the 3D machining models are computationally expensive due to the large number of SPH particles in the model. To reduce the simulation time, researchers increase the cutting speed by a factor of the actual cutting speed. Stenberg et al. [38] doubled the cutting speed to 600 m/min to reduce the simulation time. Espinosa et al. [39] increased the speed by ten times ( $10\times$ ) of the actual cutting speed to eliminate the numerical instability of the SPH method. To validate this approach, a parametric study is conducted using the 2D machining model. In this study, the cutting speed is increased by five times ( $5\times$ ),  $10\times$ , and  $20\times$  of the actual speed, and the deviation of force at a higher speed is compared with that obtained at the actual speed. Cutting forces for these speeds is plotted in Figure 8. Increasing the speed up to  $10\times$  has no significant influence on steady state cutting force. However, the chip curls less at  $10\times$  speed than at actual and at  $5\times$  cutting speeds. Thus, all further simulations are performed at  $5\times$  (five times of actual cutting speed). With large increase in cutting speed, the strain rates increase significantly, leading to the increased flow stress and hence higher cutting force.

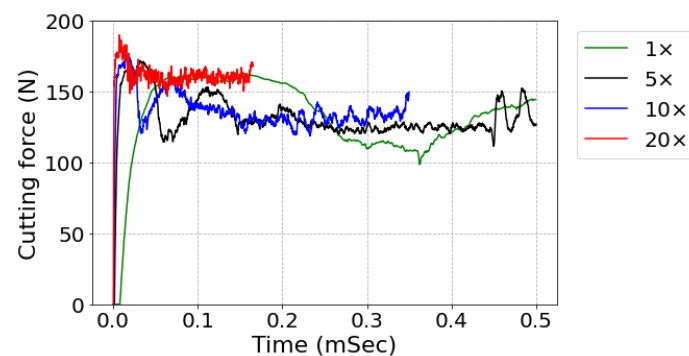
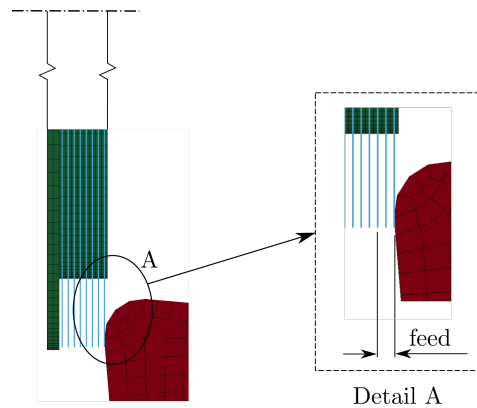


Figure 8. Cutting force comparison at different speeds for 2D model. To reduce the simulation time, evaluation of the effect of increasing cutting speeds on the simulated cutting force is performed.

### 6.2. Convergence Study for 3D Machining Model

A convergence study for three-dimensional machining model is conducted by increasing the number of SPH particles in the model. Cutting force and the chip profile are considered as the parameters for the convergence. The terminology followed is that the number of rows of SPH in feed direction/revolution is taken as a measure of the number of SPH particles. For example, 2.0 particles (shown in Figure 9) denotes that the tool will cut the first two rows of particles and touch the third row after one revolution of the workpiece. The models with 1.0 particles, 1.5 particles, 2.0 particles and 2.5 particles are simulated for the convergence study.



**Figure 9.** Terminology used for quantifying the number of SPH particles. This figure shows 2.0 particles model. In one revolution of the workpiece, the tool feed equals two rows of SPH particles in axial direction.

The plot of the cutting forces is shown in Figure 10. For a smaller number of particles, the cutting force fluctuates and does not reach a steady state. This fluctuation is the most for the 1.0 particle model and reduces for the model with the higher number of SPH particles. The cutting force converges for the 2.0 particle model and 2.5 particle model. Similar observations are made from the comparison of the chips formed by the different models. While the small chips are observed for the 1.0 particle model, the long, continuous chips are observed for the 2.0 particle model and 2.5 particle models. Thus, the 2.0 particle model is taken as the model with the converged result, which has inter-spacing between the SPH particles of 0.127 mm.

The computation time for each of these models are provided in Table 5. Clearly, the simulation time increases drastically with the increase of the number of SPH particles. With SPH model alone, the simulation time will be far from being practical. Additionally, conducting this full-scale 3D simulation with FE method is extremely challenging due to its underlying limitations. This underscores the significance of the using coupling of SPH with FE method for machining simulations.

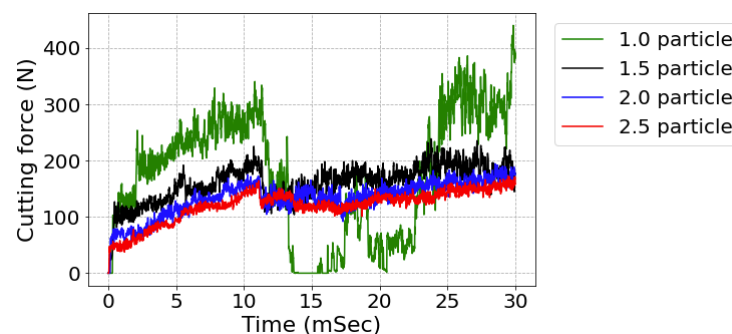


**Figure 10.** Plot for cutting force predicted by 3D machining model with different SPH particle density. This is done to achieve mesh convergence.

**Table 5.** Convergence study: Number of SPH particles and the simulation time.

Particle/Feed	Number of Particles	Run Time	Processors
1.0	43,708	7.25 h	144
1.5	101,952	24.50 h	144
2.0	192,280	64.75 h	144
2.5	323,232	183.50 h	144

6.3. 3D Machining Simulation

The results of 3D machining model is presented in this section. The results consist of the predicted cutting forces and chip morphologies. A comparison of the simulated cutting forces in all three directions with the experimental values is shown in Figure 11. As the tool approaches the workpiece, the cutting area of the workpiece increases. This leads to an increase in the cutting forces. The forces stabilize as the cutting area becomes constant after some time.

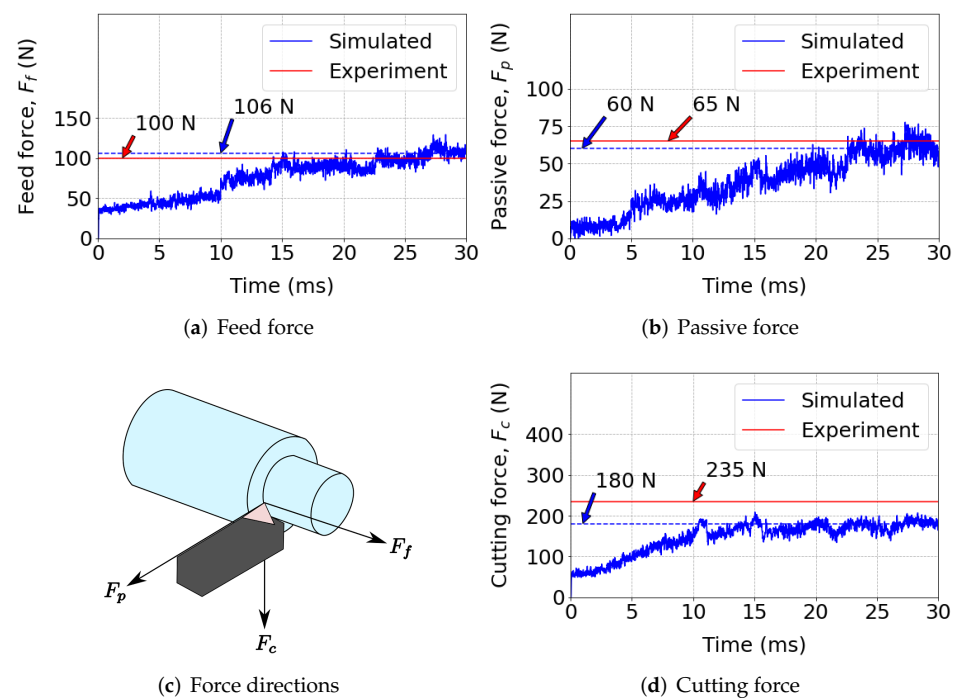


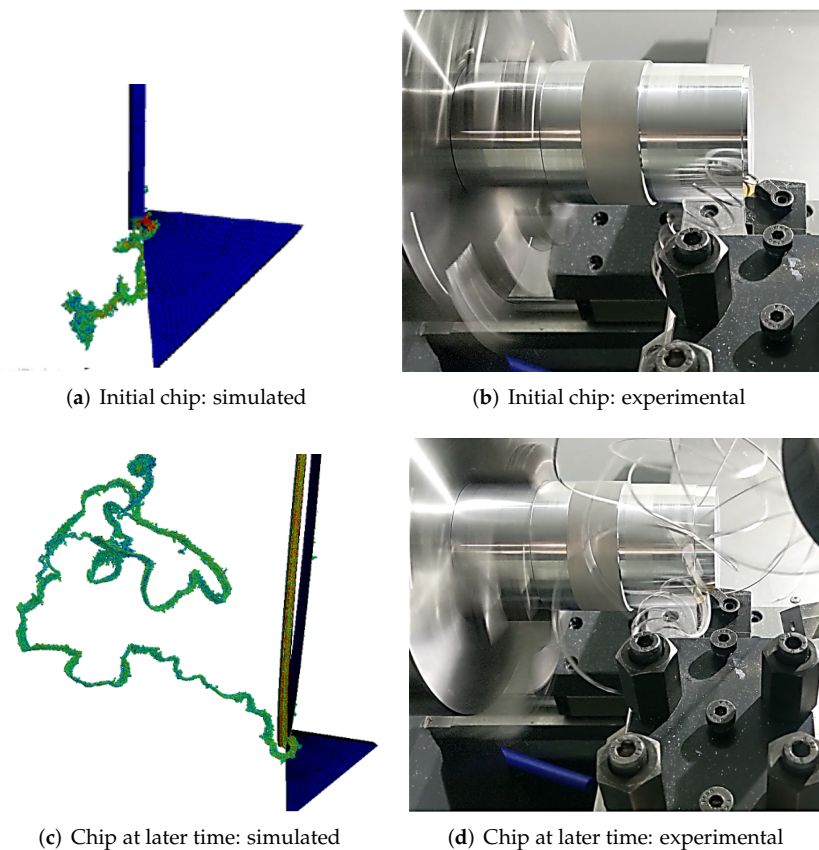
**Figure 11.** A comparison of Cutting forces predicted by 3D machining model with experimental observations.

The simulated cutting forces are summarized and compared with the experimental values in Table 6. While the feed and passive forces match well with the experiment values, the cutting force is under-predicted by 23%. The difference between the total simulated force and experimental value is  $\sim -17\%$ . Various factors, such as the uncertainties in the values of the material model parameters [40,41], value of the friction coefficient [42] and measurement uncertainties may contribute to this deviation.

**Table 6.** Comparison of forces predicted by 3D model with experiments.

	Experimental (N)	Simulated (N)
Feed Force ( $F_f$ )	100	106
Passive Force ( $F_p$ )	65	60
Cutting Force ( $F_c$ )	235	180
Total Force ( $F$ )	264	219

A comparison of the chip shape predicted by the simulation with the experiment is shown in Figure 12. At the initial time, the direction of chip formation matches with the experimental observations (Figure 12a,b). A long continuous chip is predicted by the simulation at a later time (Figure 12c,d). Accurate predictions of chip movement are useful for designing chip breakers/guards for safety while machining.

**Figure 12.** Comparison of simulated chip morphology with experimental chip at initial and later times.

Friction at the tool–chip interface is modelled using a Coulomb friction model. The value of friction coefficient ( $\mu$ ) is taken as 0.17 in the initial model. Madaj and Piška [43] used this value for the orthogonal simulation of machining of Al 2024 using the SPH method. However, using this value, the simulated feed and passive forces are significantly less compared to the experimental observations, as shown in Table 7. Thereafter, a model with the value of friction coefficient of 0.5 is simulated. This value is close to the calculated friction coefficient value of 0.57, calculated using Merchant's circle diagram [44] using the force values obtained from the turning experiment conducted for this work. Merchant's circle diagram is the most commonly used method for analysing the forces for orthogonal

machining. The forces obtained from this simulation agree well with the experimental observations. This underlines the importance of friction in modelling machining.

**Table 7.** Comparison of simulated (Sim.) cutting force with different friction coefficients ( $\mu$ ) vs. experimental values.

	Experiment (N)	Sim. (N) ( $\mu = 0.17$ )	Sim. (N) ( $\mu = 0.50$ )
Feed Force ( $F_f$ )	100	45	106
Passive Force ( $F_p$ )	65	10	60
Cutting Force ( $F_c$ )	235	210	180
Total Force ( $F$ )	264	215	219

## 7. Conclusions

This work presents a full-scale three-dimensional turning model using a coupled Smoothed Particle Hydrodynamics (SPH) method and Finite Element Method (FEM). The model is validated with the experiments by comparing the predicted cutting forces and the chip morphology. Based on the results, the following conclusions can be made:

1. The simplified two-dimensional orthogonal, plane-strain model for the actual turning operation underpredicts the cutting force and the feed force. Additionally, the 2D model cannot predict the passive force. This necessitates the use of three-dimensional machining models.
2. The forces predicted by the three-dimensional model are considerably close to the experimental values. The chip morphology also correlates with experiments in terms of the direction of the chip movement and the “long” continuous chips observed while turning Al 6061.
3. The value of friction coefficient between the tool and the workpiece has a significant influence on the simulated cutting forces, especially on the feed and passive force components. The feed cutting force governs the stability of the machining conditions. Hence, correct prediction of this force is important.
4. The benefits of using the coupling of Smoothed Particle Hydrodynamics (SPH) and Finite Element Method (FEM) are successfully demonstrated in modelling of turning operation. The challenges associated with using the FE method such as mesh distortions and material separation modelling are easily handled by the SPH method. At the same time, the high computational times associated with SPH method are reduced with the use of the FE mesh in the low deformation zones.

During turning operations, tool machines the workpiece in multiple passes, leaving behind machined surface at each pass. The model presented in this work has the advantages of no element deletion at the machined surface and reasonable computation time. Because of these advantages, this full-scale three-dimensional machining model has potential applications in simulating complex machining phenomena such as machining dynamics and tool path modulation. Furthermore, the coupling of SPH and FE methods can also be applied to simulate other machining operations such as milling and drilling more realistically. Future studies may focus on investigation of shear mechanisms by a comparison of chip geometries of experimentally observed chips and simulated chips using the proposed model.

**Author Contributions:** Conceptualization, N.O., R.C., H.P.C., T.L.S., K.T.D. and A.W.J.; Formal analysis, N.O.; Funding acquisition, K.T.D. and A.W.J.; Investigation, N.O. and R.C.; Methodology, N.O.; Supervision, H.P.C. and T.L.S.; Validation, R.C.; Writing—original draft, N.O., R.C. and K.T.D.; Writing—review & editing, H.P.C., T.L.S. and A.W.J. All authors have read and agreed to the published version of the manuscript.

**Funding:** This work was performed under the auspices of the U.S. Department of Energy by Lawrence Livermore National Laboratory under Contract DE-AC52-07NA27344, LLNL-JRNL-831826.

**Data Availability Statement:** Not applicable.

**Conflicts of Interest:** The authors declare that there is no conflict of interests regarding the publication of this work.

## References

1. Sadeghifar, M.; Sedaghati, R.; Jomaa, W.; Songmene, V. A comprehensive review of finite element modeling of orthogonal machining process: Chip formation and surface integrity predictions. *Int. J. Adv. Manuf. Technol.* **2018**, *96*, 3747–3791. [[CrossRef](#)]
2. Ivester, R.W.; Kennedy, M. *Comparison of Machining Simulations for 1045 Steel to Experimental Measurements*; Society of Manufacturing Engineers: Southfield, MI, USA, 2000.
3. Arrazola, P.; Özel, T.; Umbrello, D.; Davies, M.; Jawahir, I. Recent advances in modelling of metal machining processes. *CIRP Ann.* **2013**, *62*, 695–718. [[CrossRef](#)]
4. Zhang, B.; Bagchi, A. Finite element simulation of chip formation and comparison with machining experiment. *J. Eng. Ind.* **1994**, *116*, 289–297. [[CrossRef](#)]
5. Mabrouki, T.; Girardin, F.; Asad, M.; Rigal, J.F. Numerical and experimental study of dry cutting for an aeronautic aluminium alloy (A2024-T351). *Int. J. Mach. Tools Manuf.* **2008**, *48*, 1187–1197. [[CrossRef](#)]
6. Carroll, J.T., III; Strenkowski, J.S. Finite element models of orthogonal cutting with application to single point diamond turning. *Int. J. Mech. Sci.* **1988**, *30*, 899–920. [[CrossRef](#)]
7. Movahhedy, M.; Gadala, M.; Altintas, Y. Simulation of the orthogonal metal cutting process using an arbitrary Lagrangian–Eulerian finite-element method. *J. Mater. Process. Technol.* **2000**, *103*, 267–275. [[CrossRef](#)]
8. Chenot, J.L.; Bernacki, M.; Bouchard, P.O.; Fourment, L.; Hachem, E.; Perchat, E. Recent and future developments in finite element metal forming simulation. In Proceedings of the 11th International Conference on Technology of Plasticity, Nagoya, Japan, 19–24 October 2014; pp. 265–293.
9. Limido, J.; Espinosa, C.; Salati, M.; Lacombe, J.L. SPH method applied to high speed cutting modelling. *Int. J. Mech. Sci.* **2007**, *49*, 898–908. [[CrossRef](#)]
10. Villumsen, M.F.; Fauerholdt, T.G. *Simulation of Metal Cutting Using Smooth Particle Hydrodynamics*; LS-DYNA Anwenderforum C-III 17; DYNAmore FEM Ingenieurdienstleistungen GmbH: Stuttgart, Germany, 2008.
11. Avachat, C.S.; Cherukuri, H.P. A Parametric Study of the Modeling of Orthogonal Machining Using the Smoothed Particle Hydrodynamics Method. In *American Society of Mechanical Engineers Digital Collection, Proceedings of the ASME 2015 International Mechanical Engineering Congress and Exposition, Houston, TX, USA, 13–19 November 2015*; American Society of Mechanical Engineers: New York, NY, USA, 2015.
12. Xi, Y.; Birmingham, M.; Wang, G.; Dargusch, M. SPH/FE modeling of cutting force and chip formation during thermally assisted machining of Ti6Al4V alloy. *Comput. Mater. Sci.* **2014**, *84*, 188–197. [[CrossRef](#)]
13. Song, H.; Pan, P.; Ren, G.; Yang, Z.; Dan, J.; Li, J.; Xiao, J.; Xu, J. SPH/FEM modeling for laser-assisted machining of fused silica. *Int. J. Adv. Manuf. Technol.* **2020**, *106*, 2049–2064. [[CrossRef](#)]
14. Mane, S.; Joshi, S.S.; Karagadde, S.; Kapoor, S.G. Modeling of variable friction and heat partition ratio at the chip-tool interface during orthogonal cutting of Ti-6Al-4V. *J. Manuf. Process.* **2020**, *55*, 254–267. [[CrossRef](#)]
15. Laakso, S.V.; Agmell, M.; Ståhl, J.E. The mystery of missing feed force—The effect of friction models, flank wear and ploughing on feed force in metal cutting simulations. *J. Manuf. Process.* **2018**, *33*, 268–277. [[CrossRef](#)]
16. Calamaz, M.; Coupard, D.; Girod, F. A new material model for 2D numerical simulation of serrated chip formation when machining titanium alloy Ti-6Al-4V. *Int. J. Mach. Tools Manuf.* **2008**, *48*, 275–288. [[CrossRef](#)]
17. Childs, T.; Rahmad, R. Modifying strain-hardening of carbon steels for improved finite element simulation of orthogonal machining. *Proc. Inst. Mech. Eng. Part B J. Eng. Manuf.* **2010**, *224*, 721–732. [[CrossRef](#)]
18. Llanos, I.; Villar, J.; Urresti, I.; Arrazola, P. Finite element modeling of oblique machining using an arbitrary Lagrangian–Eulerian formulation. *Mach. Sci. Technol.* **2009**, *13*, 385–406. [[CrossRef](#)]
19. Olleak, A.; Özel, T. 3D finite element modeling based investigations of micro-textured tool designs in machining titanium alloy Ti-6Al-4V. *Procedia Manuf.* **2017**, *10*, 536–545. [[CrossRef](#)]
20. Özel, T.; Llanos, I.; Soriano, J.; Arrazola, P.J. 3D finite element modelling of chip formation process for machining Inconel 718: Comparison of FE software predictions. *Mach. Sci. Technol.* **2011**, *15*, 21–46. [[CrossRef](#)]
21. Shi, B.; Elsayed, A.; Damir, A.; Attia, H.; M’Saoubi, R. A hybrid modeling approach for characterization and simulation of cryogenic machining of Ti-6Al-4V alloy. *J. Manuf. Sci. Eng.* **2019**, *141*. [[CrossRef](#)]
22. Liu, G.; Huang, C.; Su, R.; Özel, T.; Liu, Y.; Xu, L. 3D FEM simulation of the turning process of stainless steel 17-4PH with differently texturized cutting tools. *Int. J. Mech. Sci.* **2019**, *155*, 417–429. [[CrossRef](#)]
23. Kyratsis, P.; Tzotzis, A.; Markopoulos, A.; Tapoglou, N. Cad-based 3d-fe modelling of aisi-d3 turning with ceramic tooling. *Machines* **2021**, *9*, 4. [[CrossRef](#)]
24. Gingold, R.A.; Monaghan, J.J. Smoothed particle hydrodynamics: Theory and application to non-spherical stars. *Mon. Not. R. Astron. Soc.* **1977**, *181*, 375–389. [[CrossRef](#)]

25. Lucy, L.B. A numerical approach to the testing of the fission hypothesis. *Astron. J.* **1977**, *82*, 1013–1024. [[CrossRef](#)]
26. Liu, G.; Liu, M.; Li, S. Smoothed particle hydrodynamics—A meshfree method. *Comput. Mech.* **2004**, *33*, 491. [[CrossRef](#)]
27. Feng, L.; Liu, G.; Li, Z.; Dong, X.; Du, M. Study on the effects of abrasive particle shape on the cutting performance of Ti-6Al-4V materials based on the SPH method. *Int. J. Adv. Manuf. Technol.* **2019**, *101*, 3167–3182. [[CrossRef](#)]
28. Steinberg, D. *Equation of State and Strength Properties of Selected Materials*; Lawrence Livermore National Laboratory Livermore: Livermore, CA, USA, 1996.
29. Johnson, G.; Holmquist, T. *Test Data and Computational Strength and Fracture Model Constants for 23 Materials Subjected to Large Strains, High Strain Rates, and High Temperatures*; Report No. LA-11463-MS; Los Alamos National Laboratory: Los Alamos, NM, USA, 1989.
30. Jo, H. *LS-DYNA Theory Manual*; LSTC: Livermore, CA, USA, 2006.
31. Ojal, N.; Cherukuri, H.P.; Schmitz, T.L.; Jaycox, A.W. A Comparison of Smoothed Particle Hydrodynamics (SPH) and Coupled SPH-FEM Methods for Modeling Machining. In *ASME International Mechanical Engineering Congress and Exposition*; American Society of Mechanical Engineers: New York, NY, USA, 2020; Volume 84485, p.V02AT02A036.
32. ASTM. *Standard ASTM B211:2012*; Standard Specification for Aluminum and Aluminum-Alloy Rolled or Cold Finished Bar, Rod, and Wire. ASTM International: West Conshohocken, PA, USA, 2012. [[CrossRef](#)]
33. ASM Material Data Sheet. ASM Aerospace Specification Metals, Inc. 2020. Available online: <http://asm.matweb.com/search/SpecificMaterial.asp?bassnum=MA6061T6> (accessed on 11 December 2020).
34. Schwer, L.E.; Windsor, C. Aluminum plate perforation: A comparative case study using Lagrange with erosion, multi-material ALE, and smooth particle hydrodynamics. In *Proceedings of the Seventh European LS-DYNA Conference*, Stuttgart, Germany, 14–15 June 2009; Volume 10.
35. Karandikar, J.M.; Schmitz, T.L.; Abbas, A.E. Spindle speed selection for tool life testing using Bayesian inference. *J. Manuf. Syst.* **2012**, *31*, 403–411. [[CrossRef](#)]
36. Tyler, C.T.; Schmitz, T.L. Examining the effects of cooling/lubricating conditions on tool wear in milling Hastelloy X. *Proc. NAMRI/SME* **2014**, *42*, 435–442.
37. ISO. *Standard ISO 3685:1993*; Tool-Life Testing with Single-Point Turning Tools. International Organization for Standardization: Geneva, Switzerland, 1993.
38. Stenberg, N.; Delić, A.; Björk, T. Using the SPH method to easier predict wear in machining. *Procedia CIRP* **2017**, *58*, 317–322. [[CrossRef](#)]
39. Espinosa, C.; Lacombe, J.L.; Limido, J.; Salaün, M.; Mabru, C.; Chieragatti, R. Modelling High Speed Machining with the SPH Method. In *Proceedings of the 10th International LS-DYNA® Users Conference*, Dearborn, MI, USA, 8–10 June 2008.
40. Umbrello, D.; M'saoubi, R.; Outeiro, J. The influence of Johnson–Cook material constants on finite element simulation of machining of AISI 316L steel. *Int. J. Mach. Tools Manuf.* **2007**, *47*, 462–470. [[CrossRef](#)]
41. Storchak, M.; Rupp, P.; Möhring, H.C.; Stehle, T. Determination of Johnson–Cook Constitutive Parameters for Cutting Simulations. *Metals* **2019**, *9*, 473. [[CrossRef](#)]
42. Özel, T. The influence of friction models on finite element simulations of machining. *Int. J. Mach. Tools Manuf.* **2006**, *46*, 518–530. [[CrossRef](#)]
43. Madaj, M.; Píška, M. On the SPH orthogonal cutting simulation of A2024-T351 alloy. *Procedia CIRP* **2013**, *8*, 152–157. [[CrossRef](#)]
44. Merchant, M.E. Basic mechanics of the metal-cutting process. *J. Appl. Mech.* **1944**, *11*, A168–A175. [[CrossRef](#)]